

VoD-3DGS: View-opacity-Dependent 3D Gaussian Splatting

Mateusz Nowak Wojciech Jarosz
Peter Chin
Dartmouth College
Hanover, New Hampshire, USA

{mateusz.m.nowak.th,wojciech.k.jarosz,Peter.Chin}@dartmouth.edu

Abstract

Reconstructing a 3D scene from images is challenging due to the different ways light interacts with surfaces depending on the viewer’s position and the surface’s material. In classical computer graphics, materials can be classified as diffuse or specular, interacting with light differently. The standard 3D Gaussian Splatting model struggles to represent view-dependent content, since it cannot differentiate an object within the scene from the light interacting with its specular surfaces, which produce highlights or reflections. In this paper, we propose to extend the 3D Gaussian Splatting model by introducing an additional symmetric matrix to enhance the opacity representation of each 3D Gaussian. This improvement allows certain Gaussians to be suppressed based on the viewer’s perspective, resulting in a more accurate representation of view-dependent reflections and specular highlights without compromising the scene’s integrity. By allowing the opacity to be view dependent, our enhanced model achieves state-of-the-art performance on Mip-Nerf, Tanks&Temples, Deep Blending, and Nerf-Synthetic datasets without a significant loss in rendering speed, achieving > 60FPS, and only incurring a minimal increase in memory used.

1. Introduction

3D reconstruction describes recovering the 3D structure from a set of images for a particular scene. It is an essential task in computer vision; given a reconstructed 3D scene, the user can generate novel, unseen views, which can further areas like robotics, autonomous driving, content generation, and Augmented Reality. As an early advancement, Structure-from-Motion [16] enabled a seamless transition from 2D images to 3D worlds. Nevertheless, these methods struggled with novel view synthesis and achieving a better understanding of complex scenes. With the rise of deep learning, NeRFs [13] offered a direct mapping from 3D positions to colors and density, allowing a compact and contin-

uous representation that enables novel view synthesis with photorealism and detail. However, even with significant improvements to the standard approach [1, 2], NeRFs still require a substantial amount of computing power to learn and render this 3D representation.

In recent years, 3D Gaussian Splatting [9] has offered a new approach to 3D reconstruction by providing a quick and efficient representation that allows for real-time rendering. As NeRF represents the scene through an implicit function, 3D Gaussian Splatting represents the scene explicitly through a collection of 3D anisotropic Gaussians, where each Gaussian is parameterized by its color, scale, rotation, opacity, and position in space. However, since 3D Gaussian Splatting uses rasterization to visualize the scene, it struggles with the photorealistic representation of various light interactions.

A plethora of solutions have appeared to extend the 3D Gaussian model through various improvements, from an improved shading function [8], novel shape representation [3, 7], and ray tracing [14] to the introduction of a machine learning model that enhances the capabilities of 3D Gaussians [18]. Nevertheless, these models either struggle with efficient rendering and fail to provide a simple and compact 3D representation, or they do not enhance the photorealism of the scene regarding light interactions.

In this paper, we present a straightforward yet effective enhancement to standard 3D Gaussian Splatting. Specifically, we extend the traditional scalar opacity model to a view-dependent function, which allows for a more effective representation of specular highlights, dynamic lighting, and other light interactions without sacrificing rendering speed, extending the photorealism of the scene. We validate our method across multiple datasets and demonstrate state-of-the-art results that achieve > 60 FPS on complex real-life scenes.

2. Related Work

In recent years, novel view synthesis has seen notable advancement from implicit models like Neural Radiance

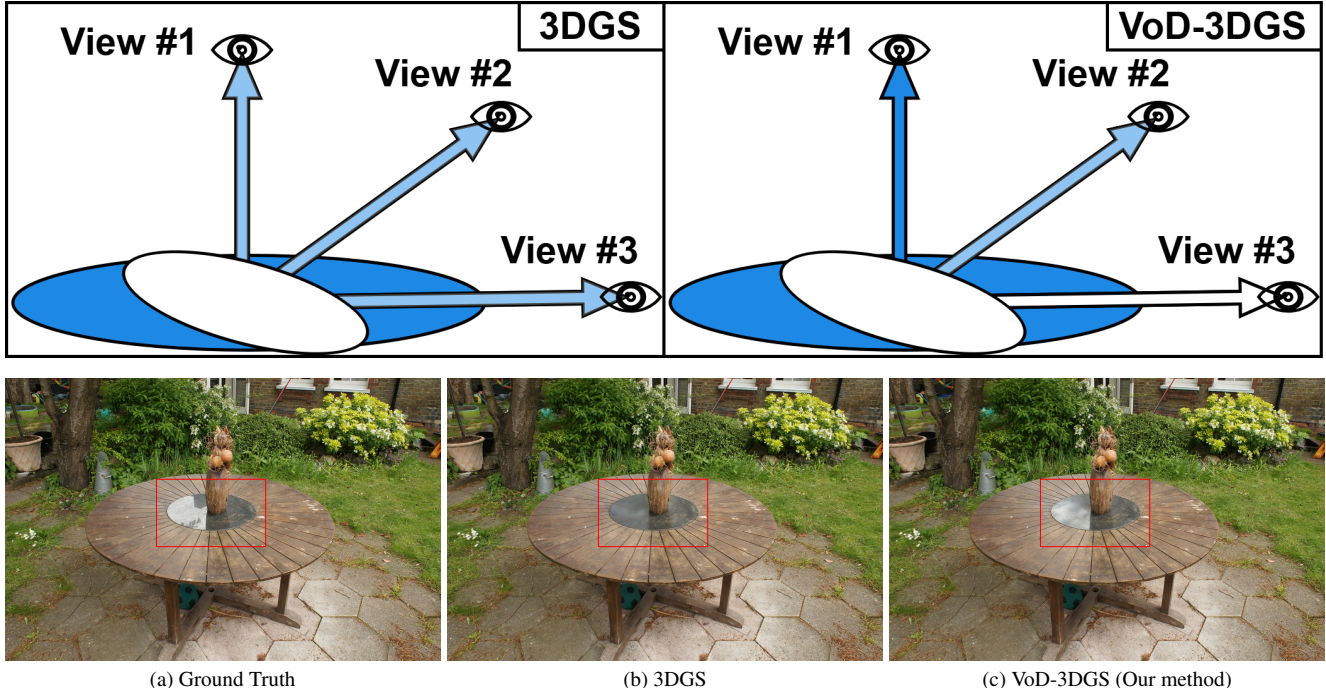


Figure 1. [Top] The visualization of the effect of our method in comparison to the standard 3D Gaussian Splatting. We can suppress or boost the impact of Gaussians responsible for modeling specular highlights and reflections for certain views by extending the opacity component of each 3D Gaussian with a symmetric matrix, acting as a learnable view-dependent factor. [Bottom] Qualitative results of our proposed method in comparison to standard 3DGS. When multiplied with the view vector, the symmetric matrix allows us to represent reflections, specular highlights, and even changing lights.

Fields (NeRF) [13], where the scene is parametrized by a multi-layer perceptron (MLP) to represent geometry and view-dependent appearance, to explicit 3D Gaussian Splatting (3DGS) [9], where geometry is represented by thousands or millions of anisotropic 3D Gaussians, whose appearances are directly stored in their representation via learnable per-Gaussian opacity and Spherical Harmonics coefficients.

2.1. Neural Radiance Fields (NeRF)

Both models have undergone further improvements, leading to reduced training times and improved quality. Instant-NGP [15] introduced a novel feature-grid-based learnable scene representation that increases the expressive power while decreasing the training time of NeRFs. Models such as Mip-NeRF [1] and Zip-NeRF [2] reduce aliasing artifacts by reasoning about sub-volumes along a cone. Additionally, to improve the visual quality of reflections and specular highlights, methods like Ref-NeRF [17] extend the NeRF model by reparameterizing the view-dependent outgoing radiance, showing the inherent lack of understanding of specular light interactions within the scene by standard NeRFs.

2.2. Modifying the material model of 3DGS

Various extensions have been proposed in the 3D Gaussian Splatting literature to modify the underlying material parameters. These extensions not only enhanced the photorealism of the scene but improved the representation of specular materials, better capturing the specular highlights and reflections. Jiang et al. [8] provided a novel normal estimation with a simplified shading function on 3D Gaussians to enhance the neural rendering in scenes with reflective surfaces. Yang et al. [18] introduced a new 3D Gaussian representation that utilizes an anisotropic spherical Gaussian (ASG) appearance field with an MLP to model the appearance of each 3D Gaussian.

We propose tackling the specular representation problem in the 3D Gaussian Splatting model without a machine learning model or an extended shading function that might negatively influence the rendering and training speed.

2.3. Modifying the shape of 3DGS

The Gaussian model was also enhanced in terms of its geometric representation. Huang et al. [7] flattened the 3D Gaussian model into anisotropic 2D Gaussian discs to better capture the underlying 3D geometry surface. Hamdi et al. [3] used the Generalized Exponential Function (GEF)

to model 3D scenes instead of the standard 3D Gaussians. Yu et al. [19] proposed to extract Gaussian Opacity Fields (GOF), by leveraging an explicit ray-Gaussian and defining the opacity of any 3D point as the minimal opacity among all training views that observed the point. Finally, Held et al. [6] utilized 3D smooth convexes as primitives for modeling radiance fields from multi-view images.

These methods show a simple paradigm in 3D Gaussian Splatting literature - we can achieve improved, more photo-realistic results with simple introductions to the underlying 3DGS model. Similarly, we propose one of these simple modifications to extend the 3D Gaussian Splatting model with a view-dependent opacity.

In this paper, we extend the 3DGS model by introducing a learnable per-Gaussian symmetric matrix. This matrix transforms the scalar opacity into a function that varies with the viewing direction, allowing for improved representation of specular highlights and reflections without any neural network introduced. Notably, this enhancement does not result in any significant increase in rendering time or memory usage.

3. Preliminaries

3.1. 3D Gaussian Splatting (3DGS)

Kerbl et al. [9] proposed parameterizing the scene with a set of learnable 3D Gaussian primitives, rendering images using differentiable rasterization through volume splatting. Each 3D Gaussian can be represented by its respective 3D covariance matrix Σ and the position of its center μ :

$$G(x) = e^{-\frac{1}{2}(x-\mu)^T \Sigma^{-1} (x-\mu)}, \quad (1)$$

where the covariance matrix $\Sigma = \mathbf{R}\mathbf{S}\mathbf{S}^T\mathbf{R}^T$ is factorized into the corresponding learnable scaling matrix \mathbf{S} and rotation matrix \mathbf{R} to guarantee positive semi-definiteness of the matrix Σ . Then, the 3D Gaussian is transformed into camera coordinates, using a viewing transformation \mathbf{W} , and projected onto the image plane, via the Jacobian of the affine approximation of the projective transformation \mathbf{J} [20]:

$$\Sigma' = \mathbf{J}\mathbf{W}\Sigma\mathbf{J}^T\mathbf{W}^T. \quad (2)$$

Projecting each of the 3D Gaussians onto a 2D plane, we obtain a 2D Gaussian representation G^{2D} , which can be efficiently sorted and then rasterized using a volumetric α blending approach, where each color C can be defined as:

$$C(p) = \sum_{i=1}^N \mathbf{c}_i \alpha_i G_i^{2D}(x) \prod_{j=1}^{i-1} (1 - \alpha_j G_j^{2D}(x)), \quad (3)$$

where the N Gaussians overlapping with the pixel p are ordered from front to back, \mathbf{c}_i is defined as the color of each

Gaussian, represented as Spherical Harmonics coefficients, and α_i is a learned per-Gaussian scalar opacity.

To optimize all the parameters of each Gaussian, the authors use standard gradient descent with a loss L defined as a combination of the L_1 color loss and a D-SSIM term, scaled with a hyperparameter λ :

$$L = (1 - \lambda)L_1 + \lambda L_{\text{D-SSIM}}. \quad (4)$$

To better reconstruct the scene, 3DGS performs an adaptive density control step, cloning Gaussians in the under-reconstructed areas and splitting Gaussians in the over-reconstructed areas. Additionally, to account for potential floaters near the camera and to help control the increase in Gaussians, the opacity values are set to a value close to zero every few thousand iterations.

3.2. The Symmetric GGX (SGGX) distribution

In the context of physically based rendering of volumes, it is important to be able to specify angularly varying properties of the medium present in the scene. Heitz et al. [5] introduced an SSGX distribution that effectively represents the spatially varying properties of anisotropic microflake participating media through a symmetric 3x3 matrix.

In the Canonical Basis, the SGGX distribution can be defined by a 3×3 symmetric positive definite matrix of six coefficients:

$$S = \begin{pmatrix} S_{xx} & S_{xy} & S_{xz} \\ S_{xy} & S_{yy} & S_{yz} \\ S_{xz} & S_{yz} & S_{zz} \end{pmatrix}, \quad (5)$$

However, the SGGX distribution can also be defined based on the projected area of the microflake in the eigenspace:

$$S = (\omega_1, \omega_2, \omega_3) \begin{pmatrix} S_{11} & 0 & 0 \\ 0 & S_{22} & 0 \\ 0 & 0 & S_{33} \end{pmatrix} (\omega_1, \omega_2, \omega_3)^T, \quad (6)$$

where $S_{11} = \sigma^2(\omega_1)$, $S_{22} = \sigma^2(\omega_2)$ and $S_{33} = \sigma^2(\omega_3)$ are positive eigenvalues that are equal to the squared projected areas of the ellipsoid in the directions given by the orthonormal eigenvectors. Given a matrix S and a direction ω_i , the projected area of the ellipsoid can be computed as:

$$\sigma(\omega_i) = \int_{\Omega} \langle \omega_i, \omega_m \rangle D(\omega_m) d\omega_m = \sqrt{\omega_i^T S \omega_i}, \quad (7)$$

where $D(\omega_m)$ is defined as the distribution of normals:

$$D(\omega_m) = \frac{1}{\pi \sqrt{|S|} (\omega_m^T S^{-1} \omega_m)^2}. \quad (8)$$

4. Method

In our paper, we propose combining the expressive capabilities of the microflake SGGX distribution with 3D Gaussian Splatting to develop a view-dependent opacity model that more accurately captures specular highlights and reflections. We will first define the new opacity model, extended by the symmetric S matrix from the SGGX distribution. Next, we will describe the new density control mechanism, which regulates the number of Gaussians through pruning and densification techniques. Then, we will propose an updated opacity rest system, responsible for minimizing the number of floaters, accounting for our extended model. Finally, we will propose a regularization loss that enforces better view consistency of our 3D Gaussians. Please see Figure 1 for a high overview of the method.

4.1. View-dependent opacity through a symmetric matrix

In the standard 3DGS implementation, the opacity of a 3D Gaussian i is defined by a learnable per-Gaussian scalar γ_i , where the final opacity α_i can be represented as:

$$\alpha_i = \sigma(\gamma_i), \quad (9)$$

where σ here denotes the sigmoid function. We propose to extend the definition of the scalar opacity α_i by introducing a symmetric matrix \hat{S}_i , parametrized with six learnable components, like the S matrix in the Canonical Basis in Eq. 5. To better capture the view-dependent light interactions, like specular highlights and reflections, without compromising the appearance of diffuse surfaces, we propose to combine both the parameter γ_i with the newly introduced matrix \hat{S}_i . The opacity function $\hat{\alpha}_i$ can be defined as:

$$\hat{\alpha}_i(\omega_{i,j}) = \sigma(\gamma_{i,j} + \omega_{i,j}^T \hat{S}_i \omega_{i,j}), \quad (10)$$

where $\omega_{i,j}$ defines the view vector between the center of the Gaussian i and the center of the camera j , allowing to define a symmetric angular distribution, similar to the SSGX distribution [5].

4.2. Density control in the view-dependent setting

In the original 3DGS paper, during the density control step of the optimization, the Gaussians were actively pruned when their opacity was lower than an introduced hyperparameter τ : $\alpha < \tau$.

To allow for opacity-based pruning within our method as well, we propose to prune the Gaussians whose maximum opacity in the training set N is lower than τ :

$$\hat{\alpha}_i(\omega_{i,j^*}) < \tau, \quad (11)$$

where $j^* = \arg \max_{j \in N} \hat{\alpha}_i(\omega_{i,j})$.

4.3. Enhanced opacity reset

In the original implementation of the paper, the opacity of the 3D Gaussians is reset to a value close to zero every few thousand iterations to minimize the number of Gaussians and lessen the impact of possible floaters. To facilitate a similar approach, we propose resetting the per-Gaussian matrix \hat{S}_i by computing its eigendecomposition and calculating a new matrix \hat{S}_i^* as either

$$\hat{S}_i = Q \begin{pmatrix} \lambda_0 & 0 & 0 \\ 0 & 0 & 0 \\ 0 & 0 & 0 \end{pmatrix} Q^{-1}, \quad \text{or} \quad \hat{S}_i = Q \begin{pmatrix} 0 & 0 & 0 \\ 0 & 0 & 0 \\ 0 & 0 & \lambda_2 \end{pmatrix} Q^{-1}, \quad (12)$$

where λ_0 and λ_2 are the highest and lowest eigenvalues respectively, and Q is a matrix of eigenvectors. We refer to these as **VoD-3DGS[L]** and **VoD-3DGS[S]** respectively in the Section 5. We decided to include both opacity resetting methods as they produce viable results in various datasets.

4.4. View consistency regularization loss

Finally, we propose to extend the loss function used for optimization in the standard 3DGS setting. We introduce a new view consistency loss L_{vc} that allows the same Gaussian, viewed from similar angles, to maintain a similar opacity.

Given a camera view i , we stochastically sample another view j , where the likelihood of selecting a specific view j is based on the number of keypoint matches between both views i and j . Then, we compute our loss L_{vc} for all the Gaussians $g \in G$ as:

$$L_{vc} = \frac{1}{|G|} \sum_{g \in G} [\max(\cos(\theta), 0) (\hat{\alpha}(\omega_{g,i}) - \hat{\alpha}(\omega_{g,j}))^2], \quad (13)$$

where θ is defined as the angle between the view vector $\omega_{g,i}$ and $\omega_{g,j}$.

Therefore, the final optimization loss can be represented as:

$$L = (1 - \lambda)L_1 + \lambda L_{D-SSIM} + L_{vc}. \quad (14)$$

5. Implementation, Evaluation and Results

5.1. Implementation

We implement our VoD-3DGS upon the original codebase of the original 3D Gaussian Splatting paper.

We do not modify any existing parameters, except for the learning rate of the γ parameter responsible for opacity learning. To learn the per-Gaussian symmetric matrix \hat{S}_i , we set the learning rate for each of the six components and the γ term to $\frac{1}{4}lr_\gamma$, where lr_γ is the original learning rate used in the 3D Gaussian Splatting paper to optimize γ .

As a preprocessing step, to create a per-view distribution for sampling views used in our view-consistency loss

L_{vc} , we use LightGlue [11] to compute keypoint matches between pairs of images. However, since standard 3D Gaussian splatting already utilizes Structure-from-Motion (SfM) [16], which also computes the information about keypoint matches between images, all the necessary information could be collected during the SfM computation.

We conduct all the experiments on a single 48GB NVIDIA L40 GPU.

5.2. Datasets

We evaluate the performance of our proposed algorithm on four datasets:

1. MipNerf-360 [1],
2. Tanks & Temples [10],
3. Deep Blending [4],
4. and NeRF-Synthetic [13].

5.3. Evaluation

We use the same training process for evaluation as 3DGS [9], using all the scenes in the MipNerf360 dataset [1], the Truck and Train scene from the Tanks & Temples dataset [10], and the Playroom and Dr. Johnson scenes from the Deep Blending dataset [4]. Additionally, we provide results on all the scenes from the NeRF-Synthetic dataset [13] to showcase our algorithm’s performance in the synthetic scenarios. We compute PSNR, SSIM, and LPIPS for each scene on the unseen testing dataset and report the mean over all the scenes used per dataset. Additionally, we report per-dataset mean FPS count, memory used, and training time for the real-life datasets.

We present our results under two names: **VoD-3DGS[S]** and **VoD-3DGS[L]**. The only distinction being whether we use the smallest or largest eigenvalue to reset the S matrix of each Gaussian (Eq. 12). The two names represent the relative memory used, where VoD-3DGS[L] has a higher memory footprint than VoD-3DGS[S].

We present our findings for the three real-life datasets in Table 1 and the synthetic dataset in Table 2. As our baselines, we use the state-of-the-art NeRF approaches (MipNerf360 [1] and Zip-Nerf [2]), 3D Gaussian Splatting [9], and 3D Gaussian Splatting methods that enhance the 3D Gaussian native model without any neural network introduced for the representation where the results are provided on the original parameters of the 3DGS (2DGS [7], GES [3], GOF [19], 3DCS [6] and GS Shader [8]). Moreover, we provide a separate evaluation of our approach on Spec-Gaussian [18] in Section 5.5.

5.4. Results

As can be seen in Table 1, our methods achieve state-of-the-art performance on all the datasets used. With the reset on the highest eigenvalue, VoD-3DGS[L] achieves the highest SSIM score in all three and the highest PSNR on the Mip-

Nerf360 and the Deep Blending dataset. As for other metrics, VoD-3DGS[L] constantly achieves the top three performance. The findings indicate that the view-dependent opacity can significantly enhance visual quality, with only slightly increased rendering time and memory used. These improvements are particularly noticeable in the specular highlights and varying lighting conditions, as demonstrated in Figures 2 and Figure 3.

Our lightweight model, VoD-3DGS[S], also achieves competitive results. Surprisingly, it even outperforms VoD-3DGS[L] on the Tanks & Temples dataset regarding PSNR. Despite its smaller size, VoD-3DGS[S] consistently ranks among the top three methods, although it falls short in the LPIPS score. As can be seen in Table 1, this method offers the best overall performance and metrics compared to other approaches.

As for the efficiency of our method, even with the trivial implementation, we can achieve real-time results, with > 60 FPS on average in all datasets, with only a slight increase in memory, significantly outperforming methods like 3DCS [6] when it comes to visual quality and speed. However, efficiency was not the main goal of this paper, and we believe there is significant room for improvement in this regard.

On the Nerf-Synthetic datasets, our methods achieved top-three scores across all statistics, as can be seen in Table 2. This time, however, VoD-3DGS[S] outperformed VoD-3DGS[L]. We believe that the smaller size of the synthetic scenes allows VoD-3DGS[S], with its stricter regularization, to identify the optimal number of 3D Gaussians needed to represent the scene without overfitting. Nonetheless, both methods deliver state-of-the-art performance on the Nerf-Synthetic datasets.

5.5. Results in comparison to Specular Gaussian

In this subsection, we evaluate our algorithm in comparison to Spec-Gaussian [18], a method that utilizes an anisotropic spherical Gaussian (ASG) appearance field with an MLP to model the appearance of each 3D Gaussian. We present our results in Table 3 over the previously mentioned real-life datasets: Mip-Nerf360, Tanks&Temples and Deep Blending.

We recompute the results from Spec-Gaussian using the same parameters as previously to achieve a fair comparison. However, since Specular Gaussian includes the anchoring technique introduced in the Scaffold-GS [12] and employs a coarse-to-fine strategy, both of which can be effectively integrated into our method, we present two sets of results - with and without these improvements.

As shown in Table 3, our performance is slightly lower than that of the full Spec-Gaussian algorithm. However, there is a significant gap between the original method and the extended Spec-Gaussian, which shows a promising fu-

Table 1. A quantitative comparison of our method was computed over three datasets compared to previous work. Our method achieves higher-quality results for all datasets in almost all the metrics for novel view synthesis while achieving > 60 FPS rendering performance with reasonable memory utilization. Results marked with † have been recomputed and ‡ have been adapted from [6], where other values have been directly adopted from the original papers. As for the training times, we report the training time with and without the keypoint pre-computation step, indicated by the number outside and in the brackets respectively.

Method	Dataset																	
	Mip-Nerf360 Dataset						Tanks & Temples						Deep Blending					
	LPIPS ↓	PSNR ↑	SSIM ↑	Train	FPS	Mem	LPIPS ↓	PSNR ↑	SSIM ↑	Train	FPS	Mem	LPIPS ↓	PSNR ↑	SSIM ↑	Train	FPS	Mem
Mip-Nerf360	0.237	27.69	0.792	48h	0.06	8.6MB	0.257	22.22	0.759	48h	0.14	8.6MB	0.245	29.40	0.901	48h	0.09	8.6MB
GES	0.250	26.91	0.794	32m	186	377MB	0.198	23.35	0.836	21m	210	222MB	0.252	29.68	0.901	30m	160	399MB
3DGS	0.214	27.21	0.815	42m	134	734MB	0.183	23.14	0.841	26m	154	411MB	0.243	29.41	0.903	36m	137	676MB
2DGS ‡	0.252	27.18	0.808	29m	64	484MB	0.212	23.13	0.831	14m	122	200MB	0.257	29.50	0.902	28m	76	353MB
3DCS	0.207	27.29	0.802	87m	25	666MB	0.157	23.95	0.851	60m	33	282MB	0.237	29.81	0.902	71m	30	332MB
3DGS †	0.215	27.53	0.816	31m (32m)	113	649MB	0.169	23.75	0.852	19m (20m)	155	372MB	0.238	29.77	0.907	31m (31m)	117	586MB
VoD-3DGS[S]	0.217	27.66	0.817	47m (73m)	78	687MB	0.165	24.17	0.859	28m (65m)	106	430MB	0.244	29.75	0.907	38m (70m)	91	559MB
VoD-3DGS[L]	0.213	27.79	0.818	53m (83m)	65	849MB	0.160	23.91	0.860	31m (71m)	84	525MB	0.240	29.84	0.908	39m (70m)	85	606MB

Table 2. A quantitative evaluation of our method compared to previous work was computed over the Nerf-Synthetic [13] dataset. Results marked with † have been recomputed, where other values have been directly adopted from the original papers.

Method	Dataset - Nerf Synthetic		
	LPIPS ↓	PSNR ↑	SSIM ↑
Mip-Nerf 360	0.060	30.34	0.951
Zip-Nerf	0.031	33.10	0.971
3DGS	0.037	33.31	0.969
GOF	0.038	33.45	0.969
GS Shader	0.029	33.38	0.968
3DGS †	0.0298	33.48	0.970
VoD-3DGS[S]	0.0296	33.79	0.971
VoD-3DGS[L]	0.0297	33.69	0.971

ture direction of our algorithm. In the case of the MipNerf-360 dataset [1], the Spec-Gaussian version without the anchoring mechanism could not fit into our memory, indicating the potential limitations of the previous work and further showcasing the benefits of both mechanisms present in the full version of Spec-Gaussian that could be incorporated into our work.

5.6. Ablations

To check the validity of our approach, we conducted an ablation study on the MipNerf-360 dataset presented in Table 4, focusing mostly on the VoD-3DGS[S] approach from our paper. We begin with the standard implementation of 3D Gaussian Splatting, as shown in the first row of the table, and extend it by incorporating the new view-dependent matrix. This involves performing an opacity reset and pruning as described in our method. However, in the second row, we do not regularize the 3D Gaussians based on view consistency. It is evident that even with only this new model, we can significantly enhance the performance compared to the standard 3D Gaussian Splatting.

In the third row of the table, we introduce the proposed

view consistency loss. Here, we sample the views used for the view consistency loss computation with uniform probability. Forcing the 3D Gaussians to have a similar opacity when viewed from similar angles slightly increases the number of Gaussians, as evident by the lower FPS count and the higher memory used. However, this change further improves the reported statistics, achieving the highest reported LPIPS and SSIM.

Finally, in the fourth row, we modify the sampling by selecting views based on the number of pairwise keypoint matches reported by LightGlue. This change shows that, by pairing the cameras with the highest visual content overlap, we can increase the PSNR even further without a significant loss to LPIPS and SSIM, removing between 10000 and 20000 Gaussians and decreasing the memory used. Given the limited scene sizes in the Nerf-Synthetic dataset [13], we believe the decrease will be more noticeable in bigger, real-life scenes like Mip-Nerf360 [1].

6. Limitations, Conclusion and Future Work

6.1. Limitations

In our paper, we acknowledge some limitations in our method. Specifically, we find that it struggles with scenes that contain less specular content. For instance, in the Tree-hill or Stump scenes from the MipNerf360 [1] dataset, our method yields slightly lower PSNR and SSIM values compared to the original method 3DGS. To address this, we could consider introducing a new regularization term aimed at minimizing the norm of the matrix \hat{S}_i . Alternatively, we could explore a different formula for calculating opacity $\hat{\alpha}_i(\omega_j)$ using the matrix \hat{S}_i and the parameter γ_i .

Additionally, we note a slight decrease in the FPS count and an increase in memory usage. Since efficiency was not the main focus of this paper, we believe there are plenty of potential enhancements from the 3D Gaussian Splatting literature that could be implemented to increase the method’s speed and reduce storage requirements.

Finally, to fully benefit from the view-dependent opac-

Table 3. A qualitative comparison of our method computed over three datasets compared to Spec-Gaussian [18]. Results marked with † have been recomputed.

Method	Dataset														
	Mip-NeRF360 Dataset					Tanks & Temples					Deep Blending				
	LPIPS ↓	PSNR ↑	SSIM ↑	FPS	Mem	LPIPS ↓	PSNR ↑	SSIM ↑	FPS	Mem	LPIPS ↓	PSNR ↑	SSIM ↑	FPS	Mem
Spec Gaussian w/o anchors †	N/A	N/A	N/A	N/A	N/A	0.140	23.26	0.855	18	1128MB	0.248	27.93	0.885	14	1666MB
Spec Gaussian †	0.190	27.97	0.817	22	776MB	0.156	24.53	0.860	45	247MB	0.226	30.33	0.906	130	187MB
VoD-GS[S]	0.217	27.66	0.817	78	687MB	0.165	24.17	0.859	106	430MB	0.244	29.75	0.907	91	559MB
VoD-GS[L]	0.213	27.79	0.818	65	849MB	0.160	23.91	0.860	84	525MB	0.240	29.84	0.908	85	606MB

Table 4. An ablation study of our method computed over the Nerf-Synthetic [13] dataset.

Method	Adjustments			Dataset - Nerf Synthetic				
	Matrix	Loss	Keypoints	LPIPS ↓	PSNR ↑	SSIM ↑	FPS	Memory
3DGS	✗	✗	✗	0.0298	33.476	0.9700	561	62MB
VoD-3DGS[S]	✓	✗	✗	0.0303	33.513	0.9699	457	64MB
	✓	✓	✗	0.0295	33.782	0.9711	394	66MB
	✓	✓	✓	0.0296	33.792	0.9710	396	65MB
VoD-3DGS[L]	✓	✓	✓	0.0297	33.690	0.9706	374	66MB

ity, our method performs the best when the pair-wise consistency loss is computed with the camera views sampled based on the visual content overlap. In this paper, we implemented the visual content matching naively, but we believe this could be seamlessly integrated with the SfM [16] pipeline, required for standard 3D Gaussian Splatting approaches.

6.2. Conclusion

The standard 3D Gaussian Splatting faces challenges in accurately representing light interactions that depend on the viewer’s perspective. We propose to address this limitation with an enhanced 3D Gaussian Splatting model by introducing a view-dependent opacity. By combining the standard scalar opacity with the square of the projected area of the SGGX [5], computed using a learnable symmetric matrix, we can more effectively capture specular highlights, reflections, and varying lighting conditions.

To ensure a consistent appearance across different views, we regularize the Gaussians through a newly introduced view consistency loss. As a result of these changes, we achieve state-of-the-art qualitative real-time performance across multiple datasets, with only a slight increase in memory usage and a negligible drop in frames per second.

However, our method comes with some limitations. Specifically, we noticed a slight decline in quality for predominantly diffuse scenes. Nevertheless, we believe that our extensions open up a promising avenue for improvement in future work.

6.3. Future Work

For future work, exploring other types of extensions to the 3D Gaussian model could lead to even greater improvements in both quality and efficiency. Additionally, with

this new extended 3D Gaussian Splatting model, we can not only introduce classical efficiency techniques associated with 3D Gaussians but also develop a new method based on our opacity matrix. Furthermore, by further separating light interaction from the scene surface, we believe a new 3D mesh reconstruction algorithm can be introduced that eliminates 3D Gaussians with highly variable opacity, leading to a higher reconstruction quality of the scene.

References

- [1] Jonathan T. Barron, Ben Mildenhall, Dor Verbin, Pratul P. Srinivasan, and Peter Hedman. Mip-nerf 360: Unbounded anti-aliased neural radiance fields. In *2022 IEEE/CVF Conference on Computer Vision and Pattern Recognition (CVPR)*, pages 5460–5469, 2022.
- [2] Jonathan T. Barron, Ben Mildenhall, Dor Verbin, Pratul P. Srinivasan, and Peter Hedman. Zip-nerf: Anti-aliased grid-based neural radiance fields. In *2023 IEEE/CVF International Conference on Computer Vision (ICCV)*, pages 19640–19648, 2023.
- [3] Abdullah Hamdi, Luke Melas-Kyriazi, Jinjie Mai, Guocheng Qian, Ruoshi Liu, Carl Vondrick, Bernard Ghanem, and Andrea Vedaldi. Ges : Generalized exponential splatting for efficient radiance field rendering. In *Proceedings of the IEEE/CVF Conference on Computer Vision and Pattern Recognition (CVPR)*, pages 19812–19822, 2024.
- [4] Peter Hedman, Julien Philip, True Price, Jan-Michael Frahm, George Drettakis, and Gabriel Brostow. Deep blending for free-viewpoint image-based rendering. *ACM Trans. Graph.*, 37(6), 2018.
- [5] Eric Heitz, Jonathan Dupuy, Cyril Crassin, and Carsten Dachsbacher. The sggx microflake distribution. *ACM Trans. Graph.*, 34(4), 2015.
- [6] Jan Held, Renaud Vandeghen, Abdullah Hamdi, Adrien Deliege, Anthony Cioppa, Silvio Giancola, Andrea Vedaldi, Bernard Ghanem, and Marc Van Droogenbroeck. 3d convex splatting: Radiance field rendering with 3d smooth convexes, 2024.
- [7] Binbin Huang, Zehao Yu, Anpei Chen, Andreas Geiger, and Shenghua Gao. 2d gaussian splatting for geometrically accurate radiance fields. In *ACM SIGGRAPH 2024 Conference Papers*, New York, NY, USA, 2024. Association for Computing Machinery.
- [8] Yingwenqi Jiang, Jiadong Tu, Yuan Liu, Xifeng Gao, Xiaoxiao Long, Wenping Wang, and Yuexin Ma. Gaussianshader: 3d gaussian splatting with shading functions for reflective surfaces. In *2024 IEEE/CVF Conference on Computer Vision and Pattern Recognition (CVPR)*, pages 5322–5332, 2024.
- [9] Bernhard Kerbl, Georgios Kopanas, Thomas Leimkuehler, and George Drettakis. 3d gaussian splatting for real-time radiance field rendering. *ACM Trans. Graph.*, 42(4), 2023.
- [10] Arno Knapitsch, Jaesik Park, Qian-Yi Zhou, and Vladlen Koltun. Tanks and temples: benchmarking large-scale scene reconstruction. *ACM Trans. Graph.*, 36(4), 2017.
- [11] Philipp Lindenberger, Paul-Edouard Sarlin, and Marc Pollefeys. Lightglue: Local feature matching at light speed. In *2023 IEEE/CVF International Conference on Computer Vision (ICCV)*, pages 17581–17592, 2023.
- [12] Tao Lu, Mulin Yu, Linning Xu, Yuanbo Xiangli, Limin Wang, Dahua Lin, and Bo Dai. Scaffold-gs: Structured 3d gaussians for view-adaptive rendering. In *2024 IEEE/CVF Conference on Computer Vision and Pattern Recognition (CVPR)*, pages 20654–20664, 2024.
- [13] Ben Mildenhall, Pratul P. Srinivasan, Matthew Tancik, Jonathan T. Barron, Ravi Ramamoorthi, and Ren Ng. Nerf: representing scenes as neural radiance fields for view synthesis. *Commun. ACM*, 65(1):99–106, 2021.
- [14] Nicolas Moenne-Loccoz, Ashkan Mirzaei, Or Perel, Riccardo de Lutio, Janick Martinez Esturo, Gavriel State, Sanja Fidler, Nicholas Sharp, and Zan Gojcic. 3d gaussian ray tracing: Fast tracing of particle scenes. *ACM Trans. Graph.*, 43(6), 2024.
- [15] Thomas Müller, Alex Evans, Christoph Schied, and Alexander Keller. Instant neural graphics primitives with a multiresolution hash encoding. *ACM Trans. Graph.*, 41(4), 2022.
- [16] Johannes L. Schönberger and Jan-Michael Frahm. Structure-from-motion revisited. In *2016 IEEE Conference on Computer Vision and Pattern Recognition (CVPR)*, pages 4104–4113, 2016.
- [17] Dor Verbin, Peter Hedman, Ben Mildenhall, Todd Zickler, Jonathan T. Barron, and Pratul P. Srinivasan. Ref-nerf: Structured view-dependent appearance for neural radiance fields. In *2022 IEEE/CVF Conference on Computer Vision and Pattern Recognition (CVPR)*, pages 5481–5490, 2022.
- [18] Ziyi Yang, Xinyu Gao, Yangtian Sun, Yihua Huang, Xiaoyang Lyu, Wen Zhou, Shaohui Jiao, Xiaojuan Qi, and Xiaogang Jin. Spec-gaussian: Anisotropic view-dependent appearance for 3d gaussian splatting. *arXiv preprint arXiv:2402.15870*, 2024.
- [19] Zehao Yu, Torsten Sattler, and Andreas Geiger. Gaussian opacity fields: Efficient adaptive surface reconstruction in unbounded scenes. *ACM Trans. Graph.*, 43(6), 2024.
- [20] Matthias Zwicker, Hanspeter Pfister, Jeroen van Baar, and Markus Gross. Ewa volume splatting. In *Proceedings of the Conference on Visualization '01*, page 29–36, USA, 2001. IEEE Computer Society.



(a) Ground Truth

(b) 3DGS

(c) VoD-3DGS[L] (Our method)

Figure 2. Comparison of our proposed method to standard 3DGS. Our method boosts the specular response in various scenes, which can be seen on the table center (Garden scene; first row), the water filter (Counter scene; fourth row), the rightmost corner of the table (Room scene; last row), and the left side of the base of the bonsai (Bonsai scene; third row). Our method also allows changing light conditions (white gravel and train tracks in the Train scene; second row).

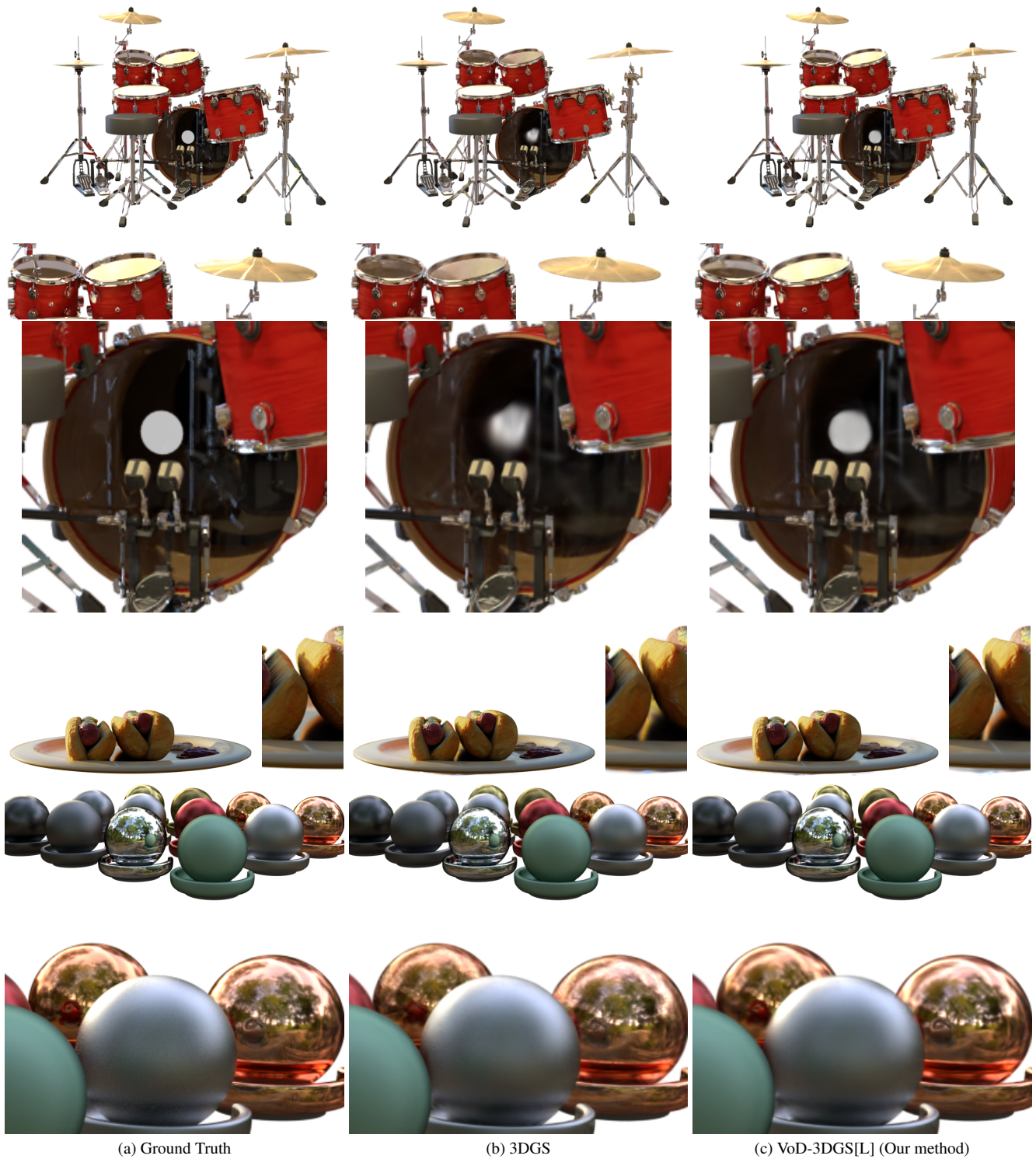


Figure 3. Our method boosts the reflection in the drums (Drums scene), on the hotdog plate (Hotdog scene), and the reflections of the red and gray spheres in the copper materials (Materials scene) of the NeRF-Synthetic [13] dataset, achieving state-of-the-art results.